Structural Amorphization-Induced Topological Order

Citian Wang,[1] Ting Cheng,[2] Zhirong Liu,[2] Feng Liu,[3,*] and Huaqing Huang[1,4,5,†]
[1]School of Physics, Peking University, Beijing 100871, China
[2]College of Chemistry and Molecular Engineering, Peking University, Beijing 100871, China
[3]Department of Materials Science and Engineering, University of Utah, Salt Lake City, Utah 84112, USA
[4]Collaborative Innovation Center of Quantum Matter, Beijing 100871, China
[5]Center for High Energy Physics, Peking University, Beijing 100871, China

(Received 24 September 2021; accepted 5 January 2022; published 2 February 2022)

Electronic properties of crystals are inherently pertained to crystalline symmetry, so that amorphization that lowers and breaks symmetry is detrimental. One important crystalline property is electron band topology which is known to be weakened and destroyed by structural disorder. Here, we report a counterintuitive theoretical discovery that atomic structural disorder by amorphization can in fact induce electronic order of topology in an otherwise topologically trivial crystal. The resulting nontrivial topology is characterized by a nonzero spin Bott index, associated with robust topological edge states and quantized conductance. The underlying topological phase transition (TPT) from a trivial crystal to a topological amorphous is analyzed by mapping out a phase diagram in the degree of structural disorder using an effective medium theory. The atomic disorder is revealed to induce topological order by renormalizing the spectral gap toward nontriviality near the phase boundary. As a concrete example, we further show such TPT in amorphous stanane by first-principles calculations. Our findings point to possible observation of an electronic ordering transition accompanied by a structural disorder transition.

DOI: 10.1103/PhysRevLett.128.056401

Introduction.—The properties of crystals are fundamentally governed by underlying crystalline symmetry. The topological states of matter, as originally established in crystalline solids, are often assessed by crystalline symmetries, such as band topology defined at high-symmetry k points [1–4]. Structural disorder is usually detrimental to topological order, because it lowers symmetry [5]. However, it has been shown that starting from a crystalline topological phase, the topological order can persist in certain amorphous regimes when the degree of disorder is small, before the atomic structural disorder eventually destroys the electronic topological order [6–20]. In this Letter, we demonstrate a counterintuitive scenario that starting from a crystalline trivial phase, topological order is actually induced by amorphization under proper conditions. This adds a new dimension to the physical origin of topological order as well as to the various existing materials' properties that can already be tailored by the unique approach of amorphization of crystalline solids [21].

It is important to note that previous studies have reported a phase transition from a trivial metal to a topological Anderson insulator (TAI) [22–26] induced by a random on-site potential disorder, which is fundamentally a many-body effect. This is because the fluctuation of on-site energies is fundamental related to on-site electron-electron interactions (the U term), which should in principle be determined by solving self-consistently a many-body Hamiltonian. The physics of the structural amorphization induced topological phase we report here is fundamentally different, because it is rooted in renormalization of spectral gap in association with single-particle energy levels, where the structural disorder is characterized with glass transition and kinetic fragility [27]. Moreover, it remains a challenge to experimentally realize the on-site Anderson disorder in realistic materials. So, instead, TAIs have only been made in artificial systems of photonic platforms [28,29], sonic crystals [30], and 1D wires of ultracold atoms [31]. In contrast, amorphous solids are ubiquitous in condensed matter [21], and nearly all materials can be principally prepared as amorphous phases [32,33] by a variety of amorphization techniques such as rapid melt quenching [34,35] (e.g., melt spinning [36], splat quenching [37], and laser glazing [38]), mechanical alloying [39,40], plasma processing [41,42], and vapor-condensation techniques [43,44]. Thus, the proposed topological phase transition (TPT) in junction with structural amorphous transition can potentially be observed experimentally with a large range of choices of materials.

We will demonstrate this surprising form of TPT from topologically trivial crystal to nontrivial amorphous by combining an effective quasilattice model with tight-binding simulations. We show that starting from a topological crystal, with increasing intensity of amorphization the system undergoes the TPT, which is characterized by a spectral gap closing and reopening process, featured with a sudden change of the topological invariant (cf. spin Bott

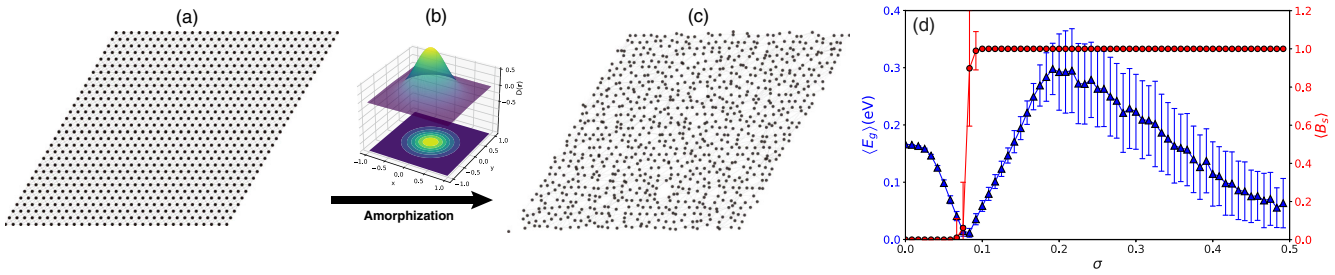

FIG. 1. Amorphization induced topological phase transition. (a) The initial triangular lattice with 900 atoms (three orbitals and two spins on each atom). The nearest and next nearest interatomic hoppings are considered. (b) Gaussian distribution of atomic displacements with random directions at $\sigma = 0.34$. (c) The quasilattice structure after amorphization. (d) Average bulk energy gap $\langle E_g \rangle$ (blue) and spin Bott index $\langle B_s \rangle$ (red) as functions of σ for 2D amorphous samples. The parameters used are $R = 1.9$ and $r_0 = 0.2$ in unit of lattice constant, $\epsilon_s = 1.8$ eV, $\epsilon_p = -6.5$ eV, $\lambda = 1.35$ eV, $V_{ss\sigma} = -0.256$ eV, $V_{sp\sigma} = 0.576$ eV, $V_{pp\sigma} = 1.152$ eV, and $V_{pp\pi} = 0.032$ eV.

index). The amorphization-induced topological state manifests also with robust edge states and quantized transport signatures. We further establish the topological phase diagram and elucidate the phase boundary at weak structural disorder based on an effective medium theory. Furthermore, using first-principles calculations, we confirm that a hydrogenated crystalline tin monolayer (the so-called stanane [45]), which is topologically trivial, becomes a topological insulator upon amorphization.

Model.—The amorphization process from perfect crystals to amorphous lattices can be rather complicated, because different approaches have been developed to synthesize amorphous materials experimentally [44,46–52] and various theoretical models have been used to generate amorphous lattices [53–60]. To investigate TPTs in amorphous lattices with different levels of structural disorder, we consider the thermal fluctuation of atoms, corresponding to a typical melt-quench process. Specifically, we adopt the quasilattice theory to capture the essential features of amorphization, which has been proved to be successful in explaining the thermodynamic properties of amorphous systems like liquids [61–67]. Our results should be general, independent of details of the amorphization model.

Starting with a perfect two-dimensional (2D) trigonal lattice as shown in Fig. 1(a), we assign random atomic displacements $\mathbf{r}$ for each atom. Assuming atoms to be held to their equilibrium positions approximately by harmonic forces, the atomic displacements follow a Gaussian distribution with random directions [68]:

$$D(\mathbf{r}) = \frac{1}{2\pi\sigma^2}\exp\left(-\frac{r^2}{2\sigma^2}\right), \tag{1}$$

where the distance standard deviation σ is scaled in unit of lattice constant a, and we choose $a = 1$ without loss of generality. In the amorphization process from melting, the variance σ^2, which represents the strength of thermal fluctuation, is approximately proportional to temperature $\sigma^2 \propto k_B T$, with k_B being the Boltzmann constant. Therefore, the intensity of structural disorder can be uniformly tuned by σ, which mimics the realistic thermal process with increasing temperature [66,67].

Based on the quasilattice model for amorphous systems, we consider a generic atomic basis tight-binding Hamiltonian with three orbitals (s, p_x, p_y) per site, which should capture the essential band topology of typical topological materials made of atoms with sp valence electrons, such as Au/GaAs(111) [69] and stanane which will be discussed later. The Hamiltonian is given by

$$H = \sum_{i\alpha}\epsilon_\alpha c^\dagger_{i\alpha}c_{i\alpha} + \sum_{\langle i\alpha, j\beta\rangle} t_{\alpha,\beta}(\mathbf{r}_{ij})c^\dagger_{i\alpha}c_{j\beta} + i\lambda\sum_i (c^\dagger_{ip_y}\sigma_z c_{ip_x} - c^\dagger_{ip_x}\sigma_z c_{ip_y}), \tag{2}$$

where $c^\dagger_{i\alpha} = (c^\dagger_{i\alpha\uparrow}, c^\dagger_{i\alpha\downarrow})$ are electron creation operators on the $\alpha(= s, p_x, p_y)$ orbital at the ith site. ϵ_α is the on-site energy of α orbital. λ is the spin-orbit coupling (SOC) strength, and σ_z is the Pauli matrix. The hopping integral $t_{\alpha,\beta}(\mathbf{r}_{ij})$, which depends on the orbital type (α and β) and the intersite vector $\mathbf{r}_{ij}$, is given by

$$t_{\alpha,\beta}(\mathbf{r}_{ij}) = \frac{\Theta(R - r_{ij})}{r_{ij}^2}\mathrm{SK}[V_{\alpha\beta\delta}, \hat{\mathbf{r}}_{ij}], \tag{3}$$

where SK[·] represents Slater-Koster parametrization for s, p_x, and p_y orbitals [70], $V_{\alpha\beta\delta}$ (with $\delta = \sigma$ or π) are the bond parameters, and $\hat{\mathbf{r}}_{ij}$ is the unit direction vector. Here, we assume the distance dependence of the hopping is captured approximately by the r^{-2} Harrison scaling law [71], and set r_{ij} to a constant $2r_0$ if the intersite distance is shorter than the effective atomic diameter $2r_0$ ignoring the compressibility of atoms. The step function Θ enforces the cutoff distance R beyond which the hopping vanishes. Since only the band inversion between s and p states of different parities is important for the realization of topological states,

we focus mainly on the 2/3 filling of electronic states hereafter.

Results.—We first calculate the bulk energy gap as a function of σ for different amorphization processes using a periodic boundary condition (PBC). For each σ, the configuration average is performed over 100 realizations of amorphous lattices. As shown in Fig. 1(d), with increasing σ, i.e., the intensity of amorphization, the energy gap first decreases to nearly zero and then increases with a transition point appearing at $\sigma = 0.09$, implying the occurrence of a TPT. When $\sigma > 0.2$, the energy gap decreases with significant fluctuations reflecting different realizations of the strongly amorphized structure. To verify the change of bulk topology during the above gap closing and reopening process, we compute the real-space topological invariant, the spin Bott index B_s, which enables the identification of quantum spin Hall (QSH) states in both crystalline and noncrystalline systems [72,73]. As shown in Fig. 1(d), the calculated spin-Bott index shows a concomitant sharp jump from 0 to 1 across the gap-closing point at $\sigma = 0.09$, confirming the TPT from a trivial crystal to a topological amorphous.

As an illustrative example of the amorphization-induced QSH state, we present the detailed results of one amorphous system with $\sigma = 0.34$ in Fig. 2. Figure 2(a) shows its energy spectrum with PBC and open boundary condition (OBC), respectively. It is found that the PBC system clearly shows an energy gap of 0.3 eV, indicating that the amorphous system is still an insulator. However, a set of eigenstates appears in the gap region of the energy spectrum for the OBC system, implying that the system becomes metallic in the presence of boundaries. In Fig. 2(b), we plotted the wave function distribution of a typical midgap state [marked as a star in Fig. 2(a). Not surprisingly, these midgap states are well localized on the boundary of the finite amorphous sample, i.e., they correspond to edge states (see also Fig. S1 in Supplemental Material [74]). Similar to the QSH state in crystals, these edge states always appear in pairs with the same energy, which are contributed from opposite spin components. All these results agree with the nonzero spin Bott index, demonstrating together the nontrivial topology of the amorphous system.

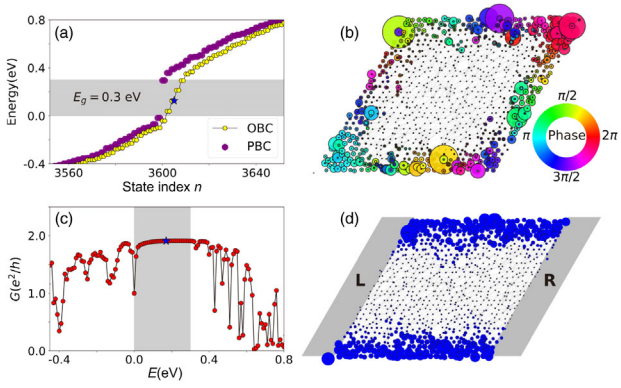

FIG. 2. Calculated results of an amorphous sample with 900 atoms at $\sigma = 0.34$. The parameters used are same as Fig 1(d) except $\lambda = 1.4$ eV. (a) Energy eigenvalues E_n versus the state index n. (b) The real-space wave function distribution of the midgap state [marked as blue star in (a)]. The size and color of the blob indicate the amplitude and phase of the wave function, respectively. (c) Two-terminal conductance G as a function of the Fermi energy E. (d) Local density of state at $E = 0.2$ eV [blue star in (c)] for the central amorphous system in the transport simulation. The size of blue dots represents the relative value of the local density of state.

We further confirm the metallic feature of the topological edge states by studying the transport properties based on the nonequilibrium Green's function method [86]. We consider a finite amorphous sample with two identical periodic leads attached to its left- and right-hand sides (see Supplemental Material [87]). As shown in Fig. 2(c), the two-terminal conductance shows a clear quantized plateau at $G = 2e^2/h$ within the bulk gap region. We further calculate the local density of state which shows the real-space distribution of conductive channels. As shown in Fig. 2(d), the local density of state of the central amorphous sample within the plateau region [e.g., $E = 0.2$ eV, as a blue star marked in Fig. 2(c)] mainly distributes at the top and bottom open edges, indicating that the quantized conductance is mostly contributed by topological edge states. These results lend additional support to our identification of the amorphous TI [6–8].

Topological phase diagram.—Having established the key signatures that an initially trivial crystal can be driven into a topological state through the amorphizing process, we now turn to the topological phase diagram for a comprehensive understanding of the necessary conditions for the amorphization-induced TPT. Since the SOC strength λ is a key factor to realize QSH states, we calculate the phase diagram in the λ-σ plane. As shown in Fig. 3, the

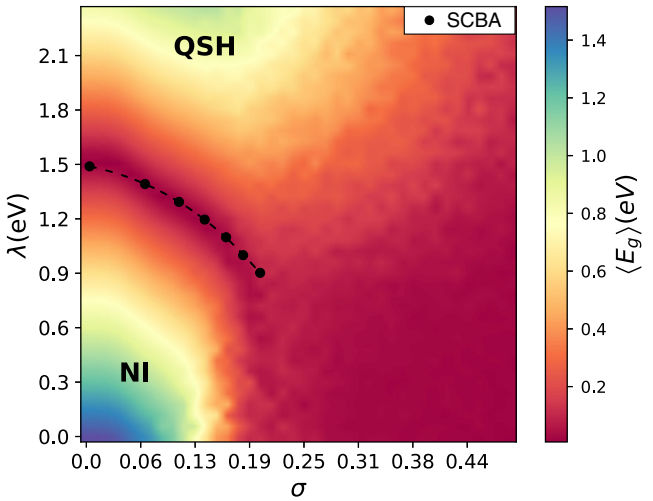

FIG. 3. Topological phase diagram in the parameter space of SOC strength λ and amorphization intensity σ. The phase boundary between the normal insulator (NI) and QSH state is a convex curve of zero energy gap, which is consistent with the analytical curve from the SCBA (dashed line).

normal insulator (NI) and QSH state are divided by an energy gap closing curve, which is confirmed by a sudden jump of spin Bott index across the phase boundary. Apparently, only for NIs with λ near the phase boundary (e.g., 1.0 eV $< \lambda <$ 1.5 eV), QSH states can be reached by amorphization. Remarkably, for a QSH state near the phase boundary, increasing σ would enhance the nontrivial gap before destroying the topological state. Another interesting point is that although sufficiently strong amorphization would eventually drive both NIs and QSH states to gapless states, the critical σ to close the bulk gap of a QSH state is much larger than that of a NI. This indicates that if one started with a topologically protected QSH state, it would be robust against structural amorphization due to a large SOC gap, although such a large gap is unlikely.

To further understand the emergence of the amorphization-driven TPT, we study the effect of structural disorder using an effective medium theory [23,25]. In the weak disorder region with small σ, amorphous systems differ from the crystal in the absence of long-range order, but the local environment remains fairly similar to the crystal. In particular, their coordination numbers are almost unchanged, albeit the discrete peaks of the radial distribution function are broadened [88–90]. Therefore, we can treat the structural disorder as perturbations to the intrinsic crystalline lattice (see Supplemental Material [74]). The effects of amorphization are taken into account as the self-energy Σ in the self-consistent Born approximation (SCBA), which is given by [91]

$$\Sigma = \langle H_d (E - H_0 - \Sigma)^{-1} H_d \rangle, \tag{4}$$

where H_0 represents the Hamiltonian of the crystalline lattice, $H_d = H - H_0$ is the Hamiltonian induced by disorder, and $\langle \cdot \rangle$ denotes the average over different amorphous configurations. It is expected that Σ would ease the band inversion for TPT by reducing the trivial gap of the effective medium Hamiltonian $H_m = H_0 + \Sigma$. For a given λ, the critical amorphization intensity σ at the phase boundary is determined by the gap-closure condition [i.e., $E_g(\lambda, \sigma) = 0$]. As shown in Fig. 3, the weak-disorder phase boundary is described quite well by the SCBA (dashed line), indicating that Σ indeed renormalizes the spectral gap.

To further gain some insight into the underlying physics, we obtain the approximate analytic solution by ignoring the variation of bond angles [92] and assuming the bond lengths are distributed uniformly in the range $(1 - \sigma, 1 + \sigma)$ [75]. For simplicity, we only consider the spin-up subspace, since the spin-up and spin-down subspaces are connected by the time-reversal symmetry. Here, H_0 represents the low-energy effective spin-up Hamiltonian around Γ with the nearest-neighbor approximation, given by

$$H_0 = \begin{pmatrix} E_s & \frac{3V_{sp\sigma}}{\sqrt{2}}(ik_x - k_y) \\ -\frac{3V_{sp\sigma}}{\sqrt{2}}(ik_x + k_y) & E_p + \lambda \end{pmatrix}, \tag{5}$$

where $E_s = \epsilon_s + 6V_{ss\sigma}$ and $E_p = \epsilon_p + 3(V_{pp\pi} + V_{pp\sigma})$ are the effective s and p levels. The self-energy Σ is estimated within the Born approximation as [74]:

$$\Sigma = \frac{18 g(\sigma)}{\lambda_0 - \lambda} \begin{pmatrix} -4V_{ss\sigma}^2 & 0 \\ 0 & (V_{pp\pi} + V_{pp\sigma})^2 \end{pmatrix}, \tag{6}$$

$$g(\sigma) = \frac{\sigma^4}{(1-\sigma^2)^2} + \frac{4\sigma^2}{3(1-\sigma^2)^3}, \tag{7}$$

where $\lambda_0 = E_s - E_p$ is the critical SOC strength in the clean limit (i.e., $\sigma = 0$). If one starts from a trivial crystal phase, i.e., $\lambda < \lambda_0$, Σ would lower the s level and raise the p level, which reduces the trivial energy gap as E_s is initially higher than E_p in our case. Namely, amorphization would promote the s-p band inversion and drive the system to a topologically nontrivial phase. On the contrary, when starting with a nontrivial phase, i.e., $\lambda > \lambda_0$, Σ would enlarge the nontrivial gap due to the sign change, which means that amorphization enhances rather than suppresses its topological protection. Thus, our analysis clearly explains the opposite behaviors of amorphization on the two sides of the phase boundary.

Material manifestation.—As a concrete material example, we study the amorphization-induced topological order in stanane, a hydrogenated α-Sn(111) monolayer which was predicted to be a topologically trivial insulator [45]. Stanane crystallizes in a buckled honeycomb lattice with two hydrogen-decorated Sn atoms per unit cell. We generate amorphous structures of stanane using a bond-flipping procedure [93,94] followed by a structural optimization based on density functional theory (see Supplemental Material [74]). This method has been proved to be efficient in constructing amorphous structures whose local structural statistics are consistent with experimentally obtained distributions for 2D amorphous systems [44,95–97]. Based on first-principles and Wannier calculations, it is found that the initially trivial stanane becomes a QSH insulator (with $B_s = 1$) displaying topological edge states after amorphization, as shown in Fig. 4. Given the experimental progress in epitaxial growth of atomically thin Sn films with atomic precision [98–102], we expect that it is experimentally feasible to realize our theoretically proposed topological order in amorphous stanane.

Three-dimensional systems.—Given the vast interest in 3D topological materials, we also investigate the possibility of amorphization-induced TPTs in 3D systems, where a structural disorder-induced transition to second-order TI phase has been shown very recently [103]. Starting with a face-centered-cubic lattice, we consider the structural

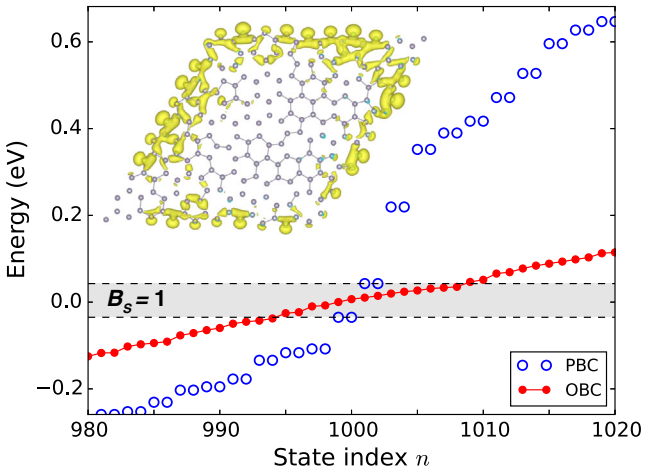

FIG. 4. The PBC and OBC energy spectrum of the amorphization-induced QSH state in stanane. The inset shows the real-space charge distribution of topological edge states.

amorphization based on Eq. (1). With increasing σ, the bulk energy gap decreases to nearly zero without reopening a gap, implying the realization of a 3D topological semimetal (Fig. S14 in Supplemental Material [74]). Remarkably, the gap closure is accompanied by a sudden jump of the spin Bott index which is related to topological spin Hall conductivity in 3D [10]. Moreover, the states around the Fermi level tend to distribute on surfaces for the topologically nontrivial amorphous structure, which is distinct from the bulk-dominated states of trivial states. These results clearly indicate the occurrence of amorphization-induced TPT in 3D.

Conclusion.—We have theoretically demonstrated a counterintuitive amorphization-induced TPT from a trivial crystalline insulator to an amorphous TI: when atoms are being disordered, electrons start to order. The resulting TI phase is confirmed by integer topological invariant, robust edge states, and quantized conductance. Amorphization is found to renormalize the spectral gap to drive the system toward the topologically nontrivial region, and hence benefit rather than harm the topological order. In addition to 2D QSH states, the amorphization induced TPT can be extendable to 3D topological states. Our findings significantly expand the horizon of a classical materials engineering approach, amorphization, to a new territory for realizing topological states, which are expected to draw immediate experimental attention. Especially, we expect a large number of topological states could be realizable by amorphizing narrow-gap semiconductors, such as Sb_2Se_3 [104], Cd_3P_2 [105,106], $Pb_{1-x}Sn_xTe$ [107,108], and $Cd_xHg_{1-x}Te$ [87,109].

This work was supported by the National Natural Science Foundation of China (Grant No. 12074006), the National Key Research and Development Program of China (No. 2021YFA1401600), and the start-up fund from Peking University. F. L. acknowledges the support of U.S. DOE-BES (Grant No. DE-FG02-04ER46148). The computational resources were supported by the high-performance computing platform of Peking University.

*fliu@eng.utah.edu
†huaqing.huang@pku.edu.cn

[1] L. Fu and C. L. Kane, Phys. Rev. B **76**, 045302 (2007).
[2] H. C. Po, A. Vishwanath, and H. Watanabe, Nat. Commun. **8**, 50 (2017).
[3] J. Cano, B. Bradlyn, Z. Wang, L. Elcoro, M. G. Vergniory, C. Felser, M. I. Aroyo, and B. A. Bernevig, Phys. Rev. Lett. **120**, 266401 (2018).
[4] Z. Song, T. Zhang, Z. Fang, and C. Fang, Nat. Commun. **9**, 3530 (2018).
[5] E. Plekhanov and C. Weber, Phys. Rev. B **100**, 115161 (2019).
[6] A. Agarwala and V. B. Shenoy, Phys. Rev. Lett. **118**, 236402 (2017).
[7] N. P. Mitchell, L. M. Nash, D. Hexner, A. M. Turner, and W. T. Irvine, Nat. Phys. **14**, 380 (2018).
[8] Q. Marsal, D. Varjas, and A. G. Grushin, Proc. Natl. Acad. Sci. U.S. A. **117**, 30260 (2020).
[9] K. Pöyhönen, I. Sahlberg, A. Weststrom, and T. Ojanen, Nat. Commun. **9**, 2103 (2018).
[10] Y.-B. Yang, T. Qin, D.-L. Deng, L.-M. Duan, and Y. Xu, Phys. Rev. Lett. **123**, 076401 (2019).
[11] I. Sahlberg, A. Weststrom, K. Pöyhönen, and T. Ojanen, Phys. Rev. Research **2**, 013053 (2020).
[12] M. N. Ivaki, I. Sahlberg, and T. Ojanen, Phys. Rev. Research **2**, 043301 (2020).
[13] B. Yang, H. Zhang, T. Wu, R. Dong, X. Yan, and X. Zhang, Phys. Rev. B **99**, 045307 (2019).
[14] S. Mansha and Y. D. Chong, Phys. Rev. B **96**, 121405(R) (2017).
[15] P. Mukati, A. Agarwala, and S. Bhattacharjee, Phys. Rev. B **101**, 035142 (2020).
[16] M. Costa, G. R. Schleder, M. Buongiorno Nardelli, C. Lewenkopf, and A. Fazzio, Nano Lett. **19**, 8941 (2019).
[17] P. Corbae, S. Ciocys, D. Varjas, S. Zeltmann, C. H. Stansbury, M. Molina-Ruiz, S. Griffin, C. Jozwiak, Z. Chen, L.-W. Wang *et al.*, arXiv:1910.13412.
[18] P. Zhou, G.-G. Liu, X. Ren, Y. Yang, H. Xue, L. Bi, L. Deng, Y. Chong, and B. Zhang, Light Sci. Appl. **9**, 133 (2020).
[19] A. G. Grushin, arXiv:2010.02851.
[20] H. Spring, A. R. Akhmerov, and D. Varjas, SciPost Phys. **11**, 022 (2021).
[21] R. Zallen, *The Physics of Amorphous Solids* (John Wiley & Sons, New York, 1998).
[22] J. Li, R.-L. Chu, J. K. Jain, and S.-Q. Shen, Phys. Rev. Lett. **102**, 136806 (2009).
[23] C. W. Groth, M. Wimmer, A. R. Akhmerov, J. Tworzydło, and C. W. J. Beenakker, Phys. Rev. Lett. **103**, 196805 (2009).
[24] H.-M. Guo, G. Rosenberg, G. Refael, and M. Franz, Phys. Rev. Lett. **105**, 216601 (2010).

[25] W. Qin, D. Xiao, K. Chang, S.-Q. Shen, and Z. Zhang, Sci. Rep. **6**, 39188 (2016).
[26] J. Song, H. Liu, H. Jiang, Q.-f. Sun, and X. C. Xie, Phys. Rev. B **85**, 195125 (2012).
[27] L. Berthier and G. Biroli, Rev. Mod. Phys. **83**, 587 (2011).
[28] S. Stützer, Y. Plotnik, Y. Lumer, P. Titum, N. H. Lindner, M. Segev, M. C. Rechtsman, and A. Szameit, Nature (London) **560**, 461 (2018).
[29] G.-G. Liu, Y. Yang, X. Ren, H. Xue, X. Lin, Y.-H. Hu, H.-x. Sun, B. Peng, P. Zhou, Y. Chong, and B. Zhang, Phys. Rev. Lett. **125**, 133603 (2020).
[30] F. Zangeneh-Nejad and R. Fleury, Adv. Mater. **32**, 2001034 (2020).
[31] E. J. Meier, F. A. An, A. Dauphin, M. Maffei, P. Massignan, T. L. Hughes, and B. Gadway, Science **362**, 929 (2018).
[32] M. H. Cohen and D. Turnbull, Nature (London) **203**, 964 (1964).
[33] D. Turnbull, Contemp. Phys. **10**, 473 (1969).
[34] P. Duwez, R. H. Willens, and W. Klement, J. Appl. Phys. **31**, 1136 (1960).
[35] H. Jones, J. Mater. Sci. **19**, 1043 (1984).
[36] A. Inoue, K. Ohtera, and T. Masumoto, Jpn. J. Appl. Phys. **27**, L736 (1988).
[37] H. Chen and D. Turnbull, Acta Mater. **18**, 261 (1970).
[38] Q. Zheng, H. Hu, M. Li, X. Tao, J. Gu, T. Wang, and Z. Li, in *Proceedings of the 1992 International Conference on Lasers and Optoelectronics*, edited by S.-S. Mei and B. Zhou, International Society for Optics and Photonics Vol. 1979 (SPIE, Bellingham, 1993), pp. 564–571, 10.1117/12.144174.
[39] L. Schultz, Mater. Sci. Eng. **97**, 15 (1988).
[40] M. S. El-Eskandarany, in *Mechanical Alloying*, edited by M. S. El-Eskandarany (William Andrew Publishing, Norwich, 2020), 3rd ed., pp. 335–416, 10.1016/C2018-0-01722-3.
[41] D. Graves, IEEE Trans. Plasma Sci. **22**, 31 (1994).
[42] G. Bruno, P. Capezzuto, and A. Madan, *Plasma Deposition of Amorphous Silicon-Based Materials* (Academic Press, San Diego, 1995).
[43] J. J. Cuomo, D. L. Pappas, J. Bruley, J. P. Doyle, and K. L. Saenger, J. Appl. Phys. **70**, 1706 (1991).
[44] C.-T. Toh, H. Zhang, J. Lin, A. S. Mayorov, Y.-P. Wang, C. M. Orofeo, D. B. Ferry, H. Andersen, N. Kakenov, Z. Guo *et al.*, Nature (London) **577**, 199 (2020).
[45] Y. Xu, B. Yan, H.-J. Zhang, J. Wang, G. Xu, P. Tang, W. Duan, and S.-C. Zhang, Phys. Rev. Lett. **111**, 136804 (2013).
[46] K. S. Suslick, S.-B. Choe, A. A. Cichowlas, and M. W. Grinstaff, Nature (London) **353**, 414 (1991).
[47] V. N. Khabashesku, J. L. Zimmerman, and J. L. Margrave, Chem. Mater. **12**, 3264 (2000).
[48] D. Tadic, F. Peters, and M. Epple, Biomaterials **23**, 2553 (2002).
[49] Z. Zeng, L. Yang, Q. Zeng, H. Lou, H. Sheng, J. Wen, D. J. Miller, Y. Meng, W. Yang, W. L. Mao, and H.-K. Mao, Nat. Commun. **8**, 322 (2017).
[50] G. Wu, X. Zheng, P. Cui, H. Jiang, X. Wang, Y. Qu, W. Chen, Y. Lin, H. Li, X. Han *et al.*, Nat. Commun. **10**, 4855 (2019).
[51] S. Hong, C.-S. Lee, M.-H. Lee, Y. Lee, K. Y. Ma, G. Kim, S. I. Yoon, K. Ihm, K.-J. Kim, T. J. Shin *et al.*, Nature (London) **582**, 511 (2020).
[52] W.-J. Joo, J.-H. Lee, Y. Jang, S.-G. Kang, Y.-N. Kwon, J. Chung, S. Lee, C. Kim, T.-H. Kim, C.-W. Yang *et al.*, Sci. Adv. **3**, e1601821 (2017).
[53] F. Wooten, K. Winer, and D. Weaire, Phys. Rev. Lett. **54**, 1392 (1985).
[54] G. T. Barkema and N. Mousseau, Phys. Rev. Lett. **77**, 4358 (1996).
[55] R. Car and M. Parrinello, Phys. Rev. Lett. **60**, 204 (1988).
[56] J. Tersoff, Phys. Rev. Lett. **61**, 2879 (1988).
[57] D. Drabold, Eur. Phys. J. B **68**, 1 (2009).
[58] A. Hannemann, J. C. Schön, M. Jansen, H. Putz, and T. Lengauer, Phys. Rev. B **70**, 144201 (2004).
[59] Y. Youn, Y. Kang, and S. Han, Comput. Mater. Sci. **95**, 256 (2014).
[60] Y. Tu, J. Tersoff, G. Grinstein, and D. Vanderbilt, Phys. Rev. Lett. **81**, 4899 (1998).
[61] J. Prins and H. Petersen, Physica (Amsterdam) **3**, 147 (1936).
[62] Y. I. Frenkel, *Kinetic Theory of Liquids* (Dover, New York, 1955).
[63] S. Bagchi, Adv. Phys. **19**, 119 (1970).
[64] S. Franchetti, Il Nuovo Cimento B **26**, 493 (1975).
[65] S. Baer, Physica (Amsterdam) **87A**, 569 (1977).
[66] N. Medvedev and Y. I. Naberukhin, Phys. Status Solidi (b) **103**, 71 (1981).
[67] B. J. Yoon, M. S. Jhon, and H. Eyring, Proc. Natl. Acad. Sci. U.S.A. **78**, 6588 (1981).
[68] V. Frechette, *Non-Crystalline Solids* (Wiley, New York, 1958).
[69] Z. Wang, K.-H. Jin, and F. Liu, Nat. Commun. **7**, 12746 (2016).
[70] J. C. Slater and G. F. Koster, Phys. Rev. **94**, 1498 (1954).
[71] W. A. Harrison, *Electronic Structure and the Properties of Solids: The Physics of the Chemical Bond* (Courier Corporation, Mineola, 2012).
[72] H. Huang and F. Liu, Phys. Rev. Lett. **121**, 126401 (2018).
[73] H. Huang and F. Liu, Phys. Rev. B **98**, 125130 (2018).
[74] See Supplemental Material at http://link.aps.org/supplemental/10.1103/PhysRevLett.128.056401 for more details about the numerical results and theoretical analysis, which includes Refs. [7,10,23,70–73,75–85].
[75] Y. Chen, E. López, S. Havlin, and H. E. Stanley, Phys. Rev. Lett. **96**, 068702 (2006).
[76] Y. Y. Atas, E. Bogomolny, O. Giraud, and G. Roux, Phys. Rev. Lett. **110**, 084101 (2013).
[77] M. L. Mehta, *Random Matrices* (Elsevier, New York, 2004).
[78] C. L. Kane and E. J. Mele, Phys. Rev. Lett. **95**, 226801 (2005).
[79] B. A. Bernevig, T. L. Hughes, and S.-C. Zhang, Science **314**, 1757 (2006).
[80] H. Ji, I. Pletikosić, Q. D. Gibson, G. Sahasrabudhe, T. Valla, and R. J. Cava, Phys. Rev. B **93**, 045315 (2016).
[81] T. J. Boyle, A. Rossi, M. Walker, P. Carlson, M. K. Miller, J. Zhao, P. Klavins, C. Jozwiak, A. Bostwick,

E. Rotenberg, V. Taufour, I. M. Vishik, and E. H. da Silva Neto, Phys. Rev. B **100**, 081105(R) (2019).
[82] M. Yang, X.-L. Zhang, and W.-M. Liu, Front. Phys. **10**, 161 (2015).
[83] G. Kresse and J. Furthmüller, Comput. Mater. Sci. **6**, 15 (1996).
[84] P. E. Blöchl, Phys. Rev. B **50**, 17953 (1994).
[85] J. P. Perdew, K. Burke, and M. Ernzerhof, Phys. Rev. Lett. **77**, 3865 (1996).
[86] S. Datta, *Electronic Transport in Mesoscopic Systems* (Cambridge University Press, Cambridge, England, 1997).
[87] E. Gornik, H. Heinrich, and L. Palmetshofer, *Physics of Narrow Gap Semiconductors* (Springer-Verlag, Berlin, Heidelberg, New York, 1982).
[88] D. Weaire, Phys. Rev. Lett. **26**, 1541 (1971).
[89] D. Weaire and M. F. Thorpe, Phys. Rev. B **4**, 2508 (1971).
[90] M. F. Thorpe, D. Weaire, and R. Alben, Phys. Rev. B **7**, 3777 (1973).
[91] P. Sheng, *Introduction to Wave Scattering, Localization, and Mesoscopic Phenomena* (Springer-Verlag, Berlin, Heidelberg, 2006).
[92] J. Zang, A. Treibergs, Y. Han, and F. Liu, Phys. Rev. Lett. **92**, 105501 (2004).
[93] M. A. Spencer and R. M. Ziff, Phys. Rev. E **93**, 042132 (2016).
[94] D. Chen, Y. Zheng, L. Liu, G. Zhang, M. Chen, Y. Jiao, and H. Zhuang, Proc. Natl. Acad. Sci. U.S.A. **118**, e2016862118 (2021).
[95] Y. Zheng, L. Liu, H. Nan, Z.-X. Shen, G. Zhang, D. Chen, L. He, W. Xu, M. Chen, Y. Jiao *et al.*, Sci. Adv. **6**, eaba0826 (2020).
[96] C. Büchner, P. Schlexer, L. Lichtenstein, S. Stuckenholz, M. Heyde, and H.-J. Freund, Z. Phys. Chem. (Frankfort/Main) **228**, 587 (2014).
[97] K. M. Burson, C. Büchner, M. Heyde, and H.-J. Freund, J. Phys. Condens. Matter **29**, 035002 (2017).
[98] F.-f. Zhu, W.-j. Chen, Y. Xu, C.-l. Gao, D.-d. Guan, C.-h. Liu, D. Qian, S.-C. Zhang, and J.-f. Jia, Nat. Mater. **14**, 1020 (2015).
[99] Y. Zang, T. Jiang, Y. Gong, Z. Guan, C. Liu, M. Liao, K. Zhu, Z. Li, L. Wang, W. Li *et al.*, Adv. Funct. Mater. **28**, 1802723 (2018).
[100] J. Deng, B. Xia, X. Ma, H. Chen, H. Shan, X. Zhai, B. Li, A. Zhao, Y. Xu, W. Duan *et al.*, Nat. Mater. **17**, 1081 (2018).
[101] M. Liao, Y. Zang, Z. Guan, H. Li, Y. Gong, K. Zhu, X.-P. Hu, D. Zhang, Y. Xu, Y.-Y. Wang *et al.*, Nat. Phys. **14**, 344 (2018).
[102] J. Falson, Y. Xu, M. Liao, Y. Zang, K. Zhu, C. Wang, Z. Zhang, H. Liu, W. Duan, K. He *et al.*, Science **367**, 1454 (2020).
[103] J.-H. Wang, Y.-B. Yang, N. Dai, and Y. Xu, Phys. Rev. Lett. **126**, 206404 (2021).
[104] H. Zhang, C.-X. Liu, X.-L. Qi, X. Dai, Z. Fang, and S.-C. Zhang, Nat. Phys. **5**, 438 (2009).
[105] P. Lin-Chung, Phys. Status Solidi (b) **47**, 33 (1971).
[106] Z. Wang, H. Weng, Q. Wu, X. Dai, and Z. Fang, Phys. Rev. B **88**, 125427 (2013).
[107] D. L. Carter and R. T. Bate, *The Physics of Semimetals and Narrow-gap Semiconductors*, Vol. 32 (Pergamon, Oxford, 1971).
[108] T. H. Hsieh, H. Lin, J. Liu, W. Duan, A. Bansil, and L. Fu, Nat. Commun. **3**, 982 (2012).
[109] T. Harman and I. Melngailis, in *Applied Solid State Science* (Elsevier, New York, 1974), Vol. 4, pp. 1–94.